

# Magnetic enhancement of $\text{Co}_{0.2}\text{Zn}_{0.8}\text{Fe}_2\text{O}_4$ spinel oxide by mechanical milling

R. N. Bhowmik\* and R. Ranganathan†

*Experimental Condensed Matter Physics Division,*

*Saha Institute of Nuclear Physics, 1/AF, Bidhannagar, Calcutta 700064, India*

S. Sarkar, C. Bansal

*School of Physics, Central University of Hyderabad, India*

R. Nagarajan

*Tata Institute of Fundamental Research, India*

## Abstract

We report the magnetic properties of mechanically milled  $\text{Co}_{0.2}\text{Zn}_{0.8}\text{Fe}_2\text{O}_4$  spinel oxide. After 24 hours milling of the bulk sample, the XRD spectra show nanostructure with average particle size  $\approx 20$  nm. The as milled sample shows an enhancement in magnetization and ordering temperature compared to the bulk sample. If the as milled sample is annealed at different temperatures for the same duration, recrystallization process occurs and approaches to the bulk structure on increasing the annealing temperatures. The magnetization of the annealed samples first increases and then decreases. At higher annealing temperature ( $\sim 1000^\circ\text{C}$ ) the system shows two coexisting magnetic phases

---

\*e-mail:rnb@cmp.saha.ernet.in

†e-mail:ranga@cmp.saha.ernet.in

*i.e.*, spin glass state and ferrimagnetic state, similar to the as prepared bulk sample. The room temperature Mössbauer spectra of the as milled sample, annealed at 300<sup>0</sup>C for different durations (upto 575 hours), suggest that the observed change in magnetic behaviour is strongly related with cations redistribution between tetrahedral (A) and octahedral (O) sites in the spinel structure. Apart from the cation redistribution, we suggest that the enhancement of magnetization and ordering temperature is related with the reduction of B site spin canting and increase of strain induced anisotropic energy during mechanical milling.

## I. INTRODUCTION

In recent years, several research groups [1–4] are involved in the investigations of nanoparticle spinel oxides because of their potential applications in magnetic devices, in micro wave technology [5], in high density magnetic recording media [6], in magnetic fluids as drug carrier etc. [4,7]. Various types of nanoparticle materials such as, metal: Fe, Co, Ni [8], metallic alloys: Fe-Cu [9], and metallic oxides: MnFe<sub>2</sub>O<sub>4</sub> [2] and ZnFe<sub>2</sub>O<sub>4</sub> [10], are under current research activity. While metal and inter metallic nanoparticles suffer from stability problems in atmospheric condition, metallic oxides are highly stable under ambient conditions [11]. Various factors such as, particle size distribution [4], inter-particle interactions [12], grain (core) and grain boundary (shell) structure [13,14] and metastable structure of the system [15] control the properties of nanoparticles. Some of the specific properties of the nanoparticles which are of interest are Quantum magnetic tunneling [4], various magnetic order like ferrimagnet/ferromagnet, spin glass/superparamagnet and spin canting effects [14,16]. The interesting aspect of magnetism in spinel oxides is that the magnetic order is strongly dependent on the competition between various superexchange type interactions *i.e.*,  $J_{AB}$  (A-O-B) and  $J_{BB}$  (B-O-B), where A: tetrahedral (A) sites moments and B: octahedral (B) sites moments, O: is O<sup>2-</sup> ions [5]. Certain amount of site disorder *i.e.*, the cations redistribution

between A and B sites is sufficient to change the super-exchange interactions in nanoparticles spinel [17,18]. Hence, the magnetic properties of the nanoparticle spinels can be drastically different from their bulk counterpart. In this light, we investigated  $\text{Co}_{0.2}\text{Zn}_{0.8}\text{Fe}_2\text{O}_4$  spinel oxide system.

The cation distribution of the bulk sample is  $(\text{Zn}_{0.8}^{2+}\text{Fe}_{0.2}^{3+})_A[\text{Co}_{0.2}^{2+}\text{Fe}_{1.8}^{3+}]_B\text{O}_4$  (A= tetrahedral sites, B= octahedral sites) [19,20]. The A site is strongly diluted with respect to B site and B site moments contribute to different size clusters. The spins inside the clusters form canted structure due to short range ferrimagnetic interactions. The total magnetization  $M$  ( $= M_B\cos\theta - M_A$ ) of such type of canted system depends not only on the sublattice (site) magnetization  $M_B$  and  $M_A$  but also on the canting angle  $\theta$  between the B site spins. The B site spin canting is strongly related with the amount of A site moments. If more number of A site moments exist in as milled  $\text{Co}_{0.2}\text{Zn}_{0.8}\text{Fe}_2\text{O}_4$  sample, the canting angle between B site spins is expected to be reduced and a drastic change in cluster glass properties of bulk sample [20] is expected. Unfortunately, most of the reports in literature concern only on the long range order system, such as  $\text{ZnFe}_2\text{O}_4$  [10] and  $\text{NiFe}_2\text{O}_4$  [14], and the magnitudes of A and B site moments but not on the short range interacting cluster glass system where change of spin canting inside the clusters plays an important role [10]. In this presentation, we show that for as milled  $\text{Co}_{0.2}\text{Zn}_{0.8}\text{Fe}_2\text{O}_4$  sample, the magnetization enhancement is related with the reduction of B site spin canting and an enhancement of ordering temperature occurs which is related with the cation redistribution and strain induced anisotropy.

## II. EXPERIMENTAL

### A. Sample preparation

Stoichiometric amounts of ZnO (99.998% from Johnson Matthey),  $\text{Fe}_2\text{O}_3$  (99.998% from Johnson Matthey) and  $\text{Co}_3\text{O}_4$  (99.5% from Fluka) oxides for the composition  $\text{Co}_{0.2}\text{Zn}_{0.8}\text{Fe}_2\text{O}_4$  were mixed and ground for 2 hours. Then, the mixture was pelletized

and sintered at  $950^{\circ}\text{C}$  for 12 hours and slowly cooled to room temperature. The pellet was again ground and pelletized and finally sintered at  $1000^{\circ}\text{C}$  for 12 hours. The heat treatment was carried out under atmospheric condition with heating and cooling rate of  $2\text{-}3^{\circ}\text{C}/\text{minute}$ . The XRD spectra of the as prepared bulk sample ( $S_0$ ) confirm formation of well crystalline cubic spinel phase. The as prepared sample was milled for 24 hours in a SPEX 8000 mixer/mill using a set of six balls, two of diameter  $1/2$  inch and four of diameter  $1/4$  inch with ball to powder weight ratio 5:1. The as milled sample ( $S_1$ ) was heat treated in air at  $300^{\circ}\text{C}$  for various durations, ranging from 2 hours to 575 hours, to study the temporal phase evolution. The 6 hours heat treated as milled samples are denoted as  $S_{N3}$  (for  $300^{\circ}\text{C}$ ),  $S_{N6}$  (for  $600^{\circ}\text{C}$ ) and  $S_{N10}$  (for  $1000^{\circ}\text{C}$ ). The heating and cooling rates were maintained at  $2\text{-}3^{\circ}\text{C}/\text{minute}$  during the heat treatment process.

## B. X-ray diffraction

The X ray diffraction (XRD) data (Fig. 1a) were taken using Philips PW1710 diffractometer with  $\text{CuK}_{\alpha}$  radiation in the  $2\theta$  range  $10^{\circ}\text{-}90^{\circ}$  with a step size  $0.02^{\circ}$ . The XRD data of as prepared bulk sample show narrow crystalline lines with estimated particle size of a few micrometers. After 24 hours milling of the bulk sample, the XRD peak lines become significantly broad and no other phases are seen, except the cubic spinel structure. The broadening in XRD lines suggest nano structure or non-uniform micro strain introduced in the lattices during milling process [21]. The width of  $< 311 >$  XRD peak line gives average particle size  $\approx 20$  nm for the as milled sample ( $S_1$ ). When the as milled sample is heat treated, the XRD lines (Fig.1b-c) become sharp, which indicates recrystallization process in the system. The average particle size increases with annealing temperature as 23 nm, 28 nm and 62 nm for the samples  $S_{N3}$ ,  $S_{N6}$  and  $S_{N10}$ , respectively. Eventhough the XRD spectrum of the  $S_{N10}$  sample is very similar to that of  $S_0$  sample, the average particle size  $\approx 62$  nm suggest that complete restoration of crystallinity close to  $S_0$  sample is yet to be reached.

### C. X-ray Fluorescence spectra

We have determined the chemical composition of S<sub>1</sub> sample by X-ray Fluorescence (XRF) technique. The Fluorescence spectrum was detected using ORTEC HPGe detector and finally recorded in a PC based multichannel analyzer. The XRF spectrum (Fig. 2) shows the characteristic K<sub>α</sub> and K<sub>β</sub> lines of Fe, Co and Zn elements. No extra lines have been found that correspond contamination from hardened steel balls with composition Fe<sub>74</sub>Cr<sub>18</sub>Ni<sub>8</sub>. The peak integrals of the K<sub>α</sub> lines of all the elements are obtained using the standard peak fitting programme to get the relative percentage. This program uses the principle of Fundamental Parameter Method [22]. The obtained composition is : Fe = 62.45%, Co = 7.17% and Zn = 30.38% which is very close to the expected values *i.e.* Fe = 63.53%, Co = 6.71% and Zn = 29.76% for Co<sub>0.2</sub>Zn<sub>0.8</sub>Fe<sub>2</sub>O<sub>4</sub> system. The maximum error of the fitted values are within 5%.

### D. Measurements

The low field dc magnetization (T = 20K to 320K, H= 10 Oe to 100 Oe) and ac susceptibility (T= 60K to 330K, h<sub>rms</sub> ≈ 1 Oe and frequency (f) = 337 Hz and 7 kHz) measurements have been performed using home made magnetometer [23]. In ZFC condition, the sample has been cooled from room temperature to 20K in the absence of dc magnetic field, then the field was applied at 20K and magnetization data were recorded while increasing the temperature. In FC condition, the sample was cooled from room temperature to 20K in presence of dc magnetic field (same magnitude which was applied during ZFC measurement) and the magnetization data were recorded with increasing temperature and keeping the field on. High field magnetization, hysteresis experiments were performed using VSM magnetometer in the fields upto ±12 Tesla in the temperature range 10K to 300K.

Mössbauer spectra were recorded at 300K without applying external magnetic field, using a constant acceleration spectrometer in transmission geometry mode. The spectra were recorded using a 5 mCi <sup>57</sup>Co in Rh matrix source. The hyperfine magnetic field (HMF)

distribution at the  $^{57}\text{Fe}$  nuclei was evaluated from the Mössbauer spectra using the method of Le Caër and Dubois [24]. In this model a linear relationship between HMF (H) and isomer shift (IS) is assumed in the form  $\text{IS} = a\text{H} + b$ , where  $a$  and  $b$  are the fitting parameters to get a minimum  $\chi^2$ . The isomer shift (IS) was calculated with respect to  $^{57}\text{Fe}$  metal.

### III. RESULTS AND DISCUSSION

#### A. AC susceptibility

Fig. 3 shows the real ( $\chi'$ ) and imaginary ( $\chi''$ ) components of ac susceptibility for sample  $S_1$ . It shows a broad  $\chi'$  maximum at  $T_B \approx 320\text{K}$  (for  $h_{rms} \approx 1\text{ Oe}$ ,  $f = 337\text{ Hz}$ ) and the corresponding  $\chi''$  maximum at  $\approx 290\text{K}$ . The broadness of the ac susceptibility maxima suggest a cluster size distribution in the as milled sample  $S_1$ . The temperature where  $\chi'$  shows maximum is defined as the average blocking temperature ( $T_B$ ) of the clusters. From the frequency dependence of ac susceptibility measurements (Fig. 3a), a positive frequency shift of  $T_B$  is observed in the  $\chi'$  as well as in the  $\chi''$  maximum in the measurement frequency range. This is a characteristic of superparamagnetic blocking of the ferromagnetic clusters in different metastable states [10]. In the low temperature region, the  $\chi'$  data show a small shoulder at  $\sim 100\text{K}$  (designated as  $T_K$ ) and  $\chi''$  data show (Fig. 3b) increasing tendency below  $T_K$ . This type of behaviour of  $T_K$  can be attributed due to the disordered surface or grain boundary spins in a nanoparticle system [14].

In order to check the effect of heat treatment on magnetic properties, we have carried out the ac susceptibility measurements for the  $S_{N10}$  sample. This heat treated sample shows mixed magnetic phases. The  $\chi'$  and  $\chi''$  data of  $S_{N10}$  sample (Fig. 4) show two magnetic ordering at  $T_{m1} \approx 70\text{K}$  and  $T_{m2} \approx 280\text{K}$  respectively. The frequency shift of  $T_f$  follows Vogel-Fulcher law

$$f = f_0 \exp^{-E_a/(T_{m1}-T_0)} \quad (1)$$

with characteristic frequency  $f_0 \approx 10^{10}$  Hz, activation energy  $E_a \approx 379$  eV and constant  $T_0 \approx 47$  K. The corresponding frequency shift per decade of  $f$  ( $\Delta T_f / T_f \Delta \log(f)$ ) is  $\approx 0.05$ , which characterizes spin glass like ordering at  $T_{m1}$  [25]. The ordering temperature at  $T_{m2}$  does not show significant frequency shift (not shown in Fig. 4), suggest ferrimagnetic ordering temperature at  $T_{m2} \approx 280$  K. The spin glass transition temperature  $T_{m1} \approx 70$  K and ferrimagnetic ordering temperature at  $T_{m2} \approx 280$  K of  $S_{N10}$  sample are slightly different with respect to the cluster spin glass freezing temperature  $T_{m1} \approx 110$  K and short range ferrimagnetic ordering temperature  $T_m \approx 260$  K for bulk sample [20]. But it is clear that the mixture of two magnetic phases (spin glass/cluster spin glass plus ferrimagnetic phase) of  $S_{N10}$  sample is very similar to the bulk sample  $S_0$ .

## B. DC magnetization

The ZFC magnetization of  $S_1$  sample (Fig. 5) shows a broad maximum at the cluster blocking temperature  $T_B \approx 320$  K ( $H \sim 30$  Oe) with a thermomagnetic irreversibility between ZFC and FC magnetization below  $T_B$ . The decrease of ZFC magnetization below  $T_B$  is due to the blocking of ferromagnetic clusters in different metastable states, whereas the FC magnetization increases below  $T_B$  due to the orientation of these ferromagnetic clusters in metastable states which give rise to more magnetic contribution [11]. It is observed (Fig. 5a and Fig. 5b) that the  $T_B$  is highly applied field dependent (*i.e.*,  $T_B \approx 320$  K, 280 K and 50 K for applied field 30 Oe, 100 Oe and 1 Tesla, respectively) as expected for superparamagnetic blocking of the clusters [11]. The superparamagnetic behaviour of the as milled sample ( $S_1$ ) can be further identified from the temperature dependence of field cooled thermoremanent magnetization (TRM) data (Fig. 5b inset) that the TRM value reduces to zero at  $T \approx T_B$ . The zero TRM value indicate that the effective inter-cluster interactions are also negligible and the clusters behave as a non-interacting small particle above  $T_B \approx 320$  K.

An interesting feature is observed when we compare the magnetization data at 100 Oe of as prepared bulk sample, as milled sample and heat treated samples (Fig. 6). The mag-

netization is enhanced when the bulk sample is milled for 24 hours. On heat treating the as milled sample, it is observed that magnetization further increases for  $S_{N3}$  sample. Then magnetization decreases for the  $S_{N6}$  sample. If the as milled sample is heat treated at higher temperature ( $S_{N10}$ ), the magnetization increases. But compared to the bulk sample  $S_0$ ,  $S_{N10}$  sample has a higher magnetization value at low temperature and lower value at temperatures  $> 200\text{K}$ . Similar non-equilibrium magnetic behaviour as a function of annealing temperature has been observed for  $\text{NiFe}_2\text{O}_4$  [27]. The superparamagnetic blocking temperature  $T_B$  (indicated in Fig. 6) decreases to 270K and 120K for  $S_{N3}$  and  $S_{N6}$ , respectively, in comparison with  $T_B \approx 280\text{K}$  for  $S_1$  sample at  $H = 100\text{ Oe}$ . The 100 Oe magnetization data of the  $S_{N10}$  sample indicate a mixture of two magnetic ordering at  $T_{m1} \approx 70\text{K}$  and  $T_{m2} \approx 225\text{K}$ , respectively, very similar to the cluster spin freezing temperature at  $T_{m1} \approx 100\text{K}$  and short range ferrimagnetic ordering temperature at  $T_{m2} \approx 230\text{K}$ , respectively, for bulk sample [20].

### C. Hysteresis

The field dependence of magnetization data (Fig. 7) under ZFC condition is similar to that of ferromagnetic isotherms but the magnetization lacks saturation even upto 12 Tesla at any temperature. This, we attribute to the spin canting effects at grain boundary [14] or superparamagnetic contribution of nanoparticles [15]. We note from Fig. 7a (inset) that the  $S_1$  sample has a better ferromagnetic behaviour in terms of saturation with respect to magnetic field which indicates that the strong spin canting behaviour of  $S_0$  sample [19,20] has decreased for the nanoparticle  $S_1$  sample. Importantly, we also note (Fig.7a, inset) that the saturation magnetization of nanoparticle sample  $S_1$  is significantly increased at room temperature with respect to the bulk sample  $S_0$ . However, the higher value of  $M$  for  $S_0$  at 10K for  $H > 4\text{T}$  compared to  $S_1$  can be understood by assuming two types of magnetic interactions in the system. One is ferromagnetic and second one is antiferromagnetic. In  $S_0$  sample the B site antiferromagnetic interactions are dominant which causes spin canting in B site and shows non-saturation in magnetization [20]. The reduction of antiferromagnetic



interactions between the B site moments gives rise the 'better' ferromagnetic behaviour, yet having a reduced saturation moment at 10K, for  $S_1$  sample. It is observed from the hysteresis loop (Fig. 7b) that isothermal remanent magnetization ( $M_R$ ), coercive field ( $H_C$ ) where  $M_R$  is zero, and irreversible field ( $H_{irr}$ ), where the hysteresis loop closes, decrease with temperature. There is no hysteresis loop at  $T \geq 290K$ . This suggest that the thermal energy close to the blocking temperature ( $\sim T_B$ ) is sufficient to reduce the coercive field to zero value [26]. The saturation magnetization ( $M_S$ ) values, obtained from  $M$  vs  $1/H$  plot, are small in comparison with the bulk sample as seen in nanocrystalline  $NiFe_2O_4$  [27]. This is possible if the B site intra-cluster spin canting decreases or if there is a redistribution of cations between A and B sites when the bulk sample is mechanically milled [28].

#### D. Mössbauer Spectroscopy

Fig. 8 shows the room temperature Mössbauer spectra in absence of any external magnetic field for the samples ( $S_0$ ),  $S_1$ ,  $S_{N3}$ ,  $S_{N6}$  and  $S_{N10}$ . The spectrum of  $S_0$  sample consists of a Lorentzian doublet arising from the  $Fe^{3+}$  ions at octahedral (B) site and a Lorentzian singlet arising from the  $Fe^{3+}$  ions at tetrahedral (A) site. The most probable cations distribution of bulk sample ( $S_0$ ) obtained is  $(Zn_{0.8}Fe_{0.2})_A[Co_{0.2}Fe_{1.8}]_BO_4$ . The isomer shift (IS) and quadrupole splitting (QS) of  $Fe^{3+}$  ions at [B] site are  $\approx +0.29$  mm/sec and 0.35 mm/sec respectively. The IS value of  $Fe^{3+}$  ions at (A) site is  $\approx -0.056$  mm/sec [20]. The Mössbauer spectrum of the bulk sample therefore confirm that  $Zn^{2+}$  ions occupy A site,  $Co^{2+}$  ions prefer B site and  $Fe^{3+}$  ions prefers both A and B sites. The Mössbauer spectrum of the  $S_1$  sample clearly indicates a hyperfine magnetic field splitting in addition to a central paramagnetic doublet. This spectrum of  $S_1$  sample represents the appearance of spontaneous magnetization of ferromagnetic clusters mixed with superparamagnetic fluctuation effect due to nanometer size of the particles [10,28]. As the annealing temperature increases, the hyperfine magnetic field splitting decreases for  $S_{N3}$  sample and the  $S_{N6}$  and  $S_{N10}$  samples show paramagnetic spectra. The Mössbauer parameters of  $S_{N10}$  sample (IS= +0.27 mm/sec and QS

$+0.43$  mm/sec for B site  $\text{Fe}^{3+}$  ions and the IS =  $+0.25$  mm/sec of A site  $\text{Fe}^{3+}$  ions) differ from that of the as prepared bulk sample which suggests that duration of heat treatment ( $\sim 6$  hours) is not enough to achieve 100% equilibrium state of the bulk samples. These results confirm that the enhancement of magnetic ordering and magnetization observed in  $S_1$  sample is intrinsic property of the material. These also further indirectly confirm the hypothesis of the presence of non-equilibrium cation distribution in the as milled sample.

To check the recovery of cation distribution from non-equilibrium state to equilibrium state, we recorded the Mössbauer spectrum of  $S_1$  sample as function of duration of heat treatment at  $300^\circ\text{C}$ . Fig. 9 shows the Mössbauer spectra and corresponding hyperfine magnetic field (HMF) distribution ( $p(H)$ ). The presence of multiple hyperfine fields at A and B site  $\text{Fe}^{3+}$  ions can be expected due to various super transferred hyperfine fields (STH) from neighbouring ions. The HMF acting on the B site  $\text{Fe}^{3+}$  ions is due to non-uniform environment, consisting of different number of  $\text{Zn}^{2+}$  and  $\text{Fe}^{3+}$  ions at the nearest neighbour A sites. The HMF experienced by the A site  $\text{Fe}^{3+}$  ions is due to nearest neighbour B site configuration [19]. It is clear from the  $p(H)$  distribution that the changes brought about by 2 hours heat treatment is not very significant but the peak intensities of hyperfine field components are decreasing and intensities of paramagnetic components are increasing for annealing time  $\geq 16$  hours. Indirectly, it gives the information that more and more number of  $\text{Zn}^{2+}$  ions stabilizing in A site with the compromise of more  $\text{Fe}^{3+}$  ions in B site. This reduces the reduction of super transferred hyperfine magnetic field via inter-sublattice superexchange interactions [19]. Fig. 10 shows the temporal evolution of the average HMF for  $300^\circ\text{C}$  heat treated sample. The solid line represent the fit data using a function of time ( $t$ ) as  $F(t) = a + b(1 - \exp(-t/t_0))$  where  $a$ ,  $b$  and  $t_0$  are constants.  $F(t)$  represents average HMF as a function of time. The fit gives a measure of the reaction kinetics through atomic diffusion as the sample gets annealed.

#### IV. SUMMARY AND CONCLUSIONS

Usually nano materials lead to the decrease in magnetization and ordering temperature as the particle size decreases [11,2]. This is already observed in  $\text{Co}_{0.2}\text{Zn}_{0.8}\text{Fe}_2\text{O}_4$  with particle size  $\sim 6\text{nm}$  to  $70\text{ nm}$ , prepared by coprecipitation method [29]. However, the bulk  $\text{Co}_{0.2}\text{Zn}_{0.8}\text{Fe}_2\text{O}_4$  sample with short range ferrimagnetic ordering temperature  $\sim 260\text{K}$  and paramagnetic at  $300\text{K}$  [20] after 24 hours mechanical milling gives nanoparticles  $\sim 20\text{ nm}$  which shows ferromagnetic cluster blocking state below  $T_B \approx 320\text{K}$  with an enhancement of magnetization. Because of the weak inter-sublattice interactions  $J_{AB}$  (due to low A site  $\text{Fe}^{3+}$  population), the B site spins form canted structure in bulk  $\text{Co}_{0.2}\text{Zn}_{0.8}\text{Fe}_2\text{O}_4$  sample. The stable cation distribution of the bulk sample is destroyed due to mechanical milling and a non-equilibrium disordered state, *i.e.* the increase of A site  $\text{Fe}^{3+}$  population enhances the inter-sublattice exchange interactions  $\text{Fe}_A^{3+}-\text{O}^{2-}-\text{Fe}_B^{3+}$  ( $J_{AB}$ ) and change the B sublattice superexchange interactions  $\text{Fe}_B^{3+}-\text{O}^{2-}-\text{Fe}_B^{3+}$ . This makes the clusters more ferromagnetic with lower spin canting. The reduction of spin canting inside the clusters enhances the magnetization. The superparamagnetic fluctuation effect is expected due to the nano size clusters (particles). The cations redistribution surely is the main factor which controls the magnetic properties of nanoparticle system but distortion of spherical shape and strain induced anisotropy energy due to mechanical milling can give rise to a preferential orientation of the spins inside the clusters.

The magnetic reversibility of the heat treated ( $S_{N10}$ ) milled sample towards the bulk sample (may not 100%, due to different micro structural parameters like particle size, cluster size distribution, spin canting angle inside the clusters) conclusively show that enhancement of magnetization and ordering temperature of the as milled samples are intrinsic property of  $\text{Co}_{0.2}\text{Zn}_{0.8}\text{Fe}_2\text{O}_4$  spinel oxide.

Acknowledgement: One of the authors RNB thanks Council of Scientific and Industrial Research (CSIR, India) for providing fellowship [F.No.9/489(30)/98-EMR-I ].

## REFERENCES

- [1] D. J. Fatemi, V. G. Harris, M. X. Chen, S. K. Malik, W. B. Yelon, G. J. Long and A. Mohan, J. Appl. Phys. **85**, 5172(1999)
- [2] J. P. Chen, C. M. Sorensen, K. J. Klabunde, G. C. Hadjipanayis, E. Devlin and A. Kostikas, Phys. Rev. B **54**, 9288(1996)
- [3] G. F. Goya and H. R. Rechenberg, J. Phys: Condens. Matter **10**, 11829(1998)
- [4] Magnetic properties of fine particles, edited by J. L. Dorman and D. Fiorani (North-Holand, 1991)
- [5] V. A. M. Brabers, Hand book of Magnetic Materials, edited by K. H. buschow **8**, 189(1995); S. Krupika and P. Novak, Ferromagnetic Materials, edited by E. P. Wolfarth, North-Holand publishing company **3**, 189(1982)
- [6] M.H. Kryder, Material Res. Bull., **21**, 17 (1996)
- [7] Scientific and Clinical Applications of Magnetic carriers, edited by U. Hfeli, W. Schitt, J. Tellet, M. Zborowski, Plenum: New York, (1997)
- [8] S. K. Khanna and S. Linderorth. Phys. Rev. Lett. **67**, 742(1991)
- [9] P. Crespo, A. Hernando and A. Garcia-Escorial, Phys. Rev. B **49**, 13227(1994)
- [10] H. H. Hamdeh, J. C. Ho, S. A. Oliver, R. J. Willey, G. Oliveri and G. Busca, J. Appl. Phys. **81**, 1851(1997)
- [11] Qi Chen and Z. J. Zhang, Appl. Phys. Lett. **73**, 3156(1998)
- [12] D. Fiorani, J. L. Dormann, R. Cherkaoui, E. Tronc, F. Lucari, F. D’Orazio, L. Spinu, M. Nogues, A. Garcia, A. M. Testa, J. Magn. Magn. Mater. **196-197**, 143(1999)
- [13] L. Bianco, A. Hernando, E. Bonetti and E. Navarro, Phys. Rev. B **56**, 8894(1997)
- [14] R. H. Kodama, A. E. Berkowitz, E. J. McNiff. Jr and S. Foner, **77**, 394(1996)

- [15] G. F. Goya, H. R. Rechenberg and J. Z. Jiang, J. Magn. Magn. Mater. **218**, 221(2000)
- [16] M. Zheng, X. C. Wu, B. S. Zou and Y. J. Wang, J. Magn. Magn. Mater. **183**, 152(1998)
- [17] V. A. M. Brabers, Phys. Rev. Lett. **68**, 3113(1992)
- [18] P. J. van der Zaag, A. Noordermeer, M. T. Johnson and P. F. Bongers, Phys. Rev. Lett. **68**, 3112(1992)
- [19] G. A. Petitt and D. W. Forester, Phys. Rev. B **4**, 3912(1971)
- [20] R. N. Bhowmik and R. Ranganathan, J. Magn. Magn. Mater. (in press)
- [21] B. D. Cillity, Elements of X-Ray Diffraction ( second edition), Addison-Wesley publishing Company, Inc(1977)
- [22] R. Jenkins, R. Gould and D. Gedcke, Quantitative X-ray Spectroscopy (Dekker, New York), 445(1981)
- [23] Anindita Ray, A. Chakravarti and R. Ranganathan, Rev. Sci. Instrum., **67**, 789 (1996)  
; A. Chakravarti , R. Ranganathan and A. K. Raychaudhuri, Pramana-J.Phys., **36**, 231 (1991)
- [24] G. Le Caër and J. M. Dubois, J. Phys. E **12**, 1083(1979)
- [25] J. A. Mydosh, Spin Glasses: An experimental Introduction (Taylor & Francis), 1993
- [26] M. Muroi, R. Street, P. G. McCormick and J. Amighian, Phy. Rev. B **63**, 184414-1(2001)
- [27] A. E. Berkowitz, J. A. Lahut, C. E. VanBuren, IEEE Transactions on Magnetism **MAG-16**, 184(1980)
- [28] C. N. Chinnasamy, A. Narayanasamy, N. Ponpandian, K. Chattopadhyay, K. Shinoda, B. Jeyadevan, K. Tohji, K. Nakatsuka, T. Furubayashi and K. Nakatani, Phy. Rev. B **63**, 184108-1(2001) **12**, 7795(2000)
- [29] S. Dey, A. Roy, J. Ghose, R. N. Bhowmik and R. Ranganathan, under communication

### Figure Caption

- Fig.1 XRD spectra for  $\text{Co}_{0.2}\text{Zn}_{0.8}\text{Fe}_2\text{O}_4$  spinel oxide heated at different temperatures. For the notation  $S_0$ ,  $S_1$ ,  $S_{N3}$ ,  $S_{N6}$  and  $S_{N10}$  see in the text.
- Fig.2 X-ray Fluorescence Spectrum for the as milled sample. the arrow indicates the corresponding metals characteristics  $K_\alpha$  and  $K_\beta$  lines.
- Fig.3 Ac susceptibility  $\chi'$  (in a) and  $\chi''$  (in b) data for as milled sample ( $S_1$ ).  $T_B$  and  $T_K$  represent blocking and spin canting temperature, respectively.
- Fig.4 Ac susceptibility  $\chi'$  (in a) and  $\chi''$  (in b) for the  $1000^\circ\text{C}$ -6 hour heat treated sample ( $S_{N10}$ ). Fig.a inset shows ac susceptibility data at 1 Oe ac field,  $f = 337$  Hz and  $\ln f$  vs  $1/T_{m1}$  plot for the same sample.
- Fig.5 Dc magnetization vs temperature for 24 hrs milled  $\text{Co}_{0.2}\text{Zn}_{0.8}\text{Fe}_2\text{O}_4$  sample. Fig. b inset shows the temperature dependence of field cooled (FC) (cooled in a field of 60 Oe) thermoremanent magnetization (TRM).
- Fig.6 Temperature dependence of dc magnetization data for different heat treated samples at 100 Oe field.
- Fig.7 a)  $M$  vs  $H$  plot at different temperatures for  $S_1$  sample and inset Fig. compare the 10K and 290K data of  $S_0$  and  $S_1$  samples. b) Hysteresis loops at different temperatures for  $S_1$  sample. For  $M_R$ ,  $H_C$  and  $H_{irr}$  see text.
- Fig.8 Room temperature Mössbauer spectra recorded in absence of field for as prepared bulk ( $S_0$ ) and heat treated as milled  $S_1$ ,  $S_{N3}$ ,  $S_{N6}$  and  $S_{N10}$  sample.
- Fig.9 Room temperature Mössbauer spectra for heat treated  $\text{Co}_{0.2}\text{Zn}_{0.8}\text{Fe}_2\text{O}_4$  sample at  $300^\circ\text{C}$  for different time (left) and corresponding hyperfine field distribution (right).
- Fig.10 Annealing time (at  $300^\circ\text{C}$ ) dependence of average hyperfine field value for as milled  $\text{Co}_{0.2}\text{Zn}_{0.8}\text{Fe}_2\text{O}_4$  sample.

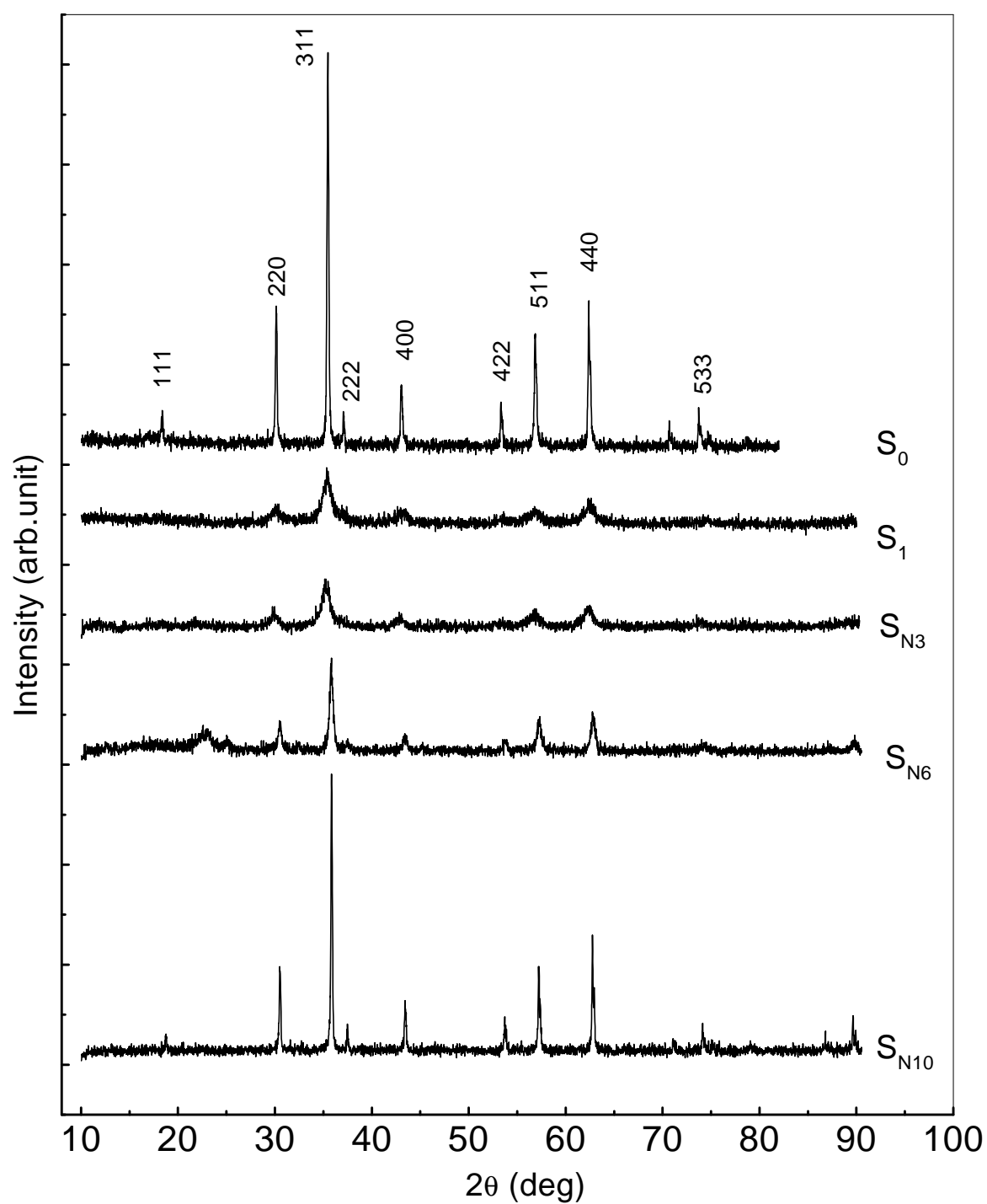


Fig.1 XRD spectra for  $\text{Co}_{0.2}\text{Zn}_{0.8}\text{Fe}_2\text{O}_4$  spinel oxide heated at different temperatures. For the notation  $S_0$ ,  $S_1$ ,  $S_{N3}$ ,  $S_{N6}$  and  $S_{N10}$  see in the text.

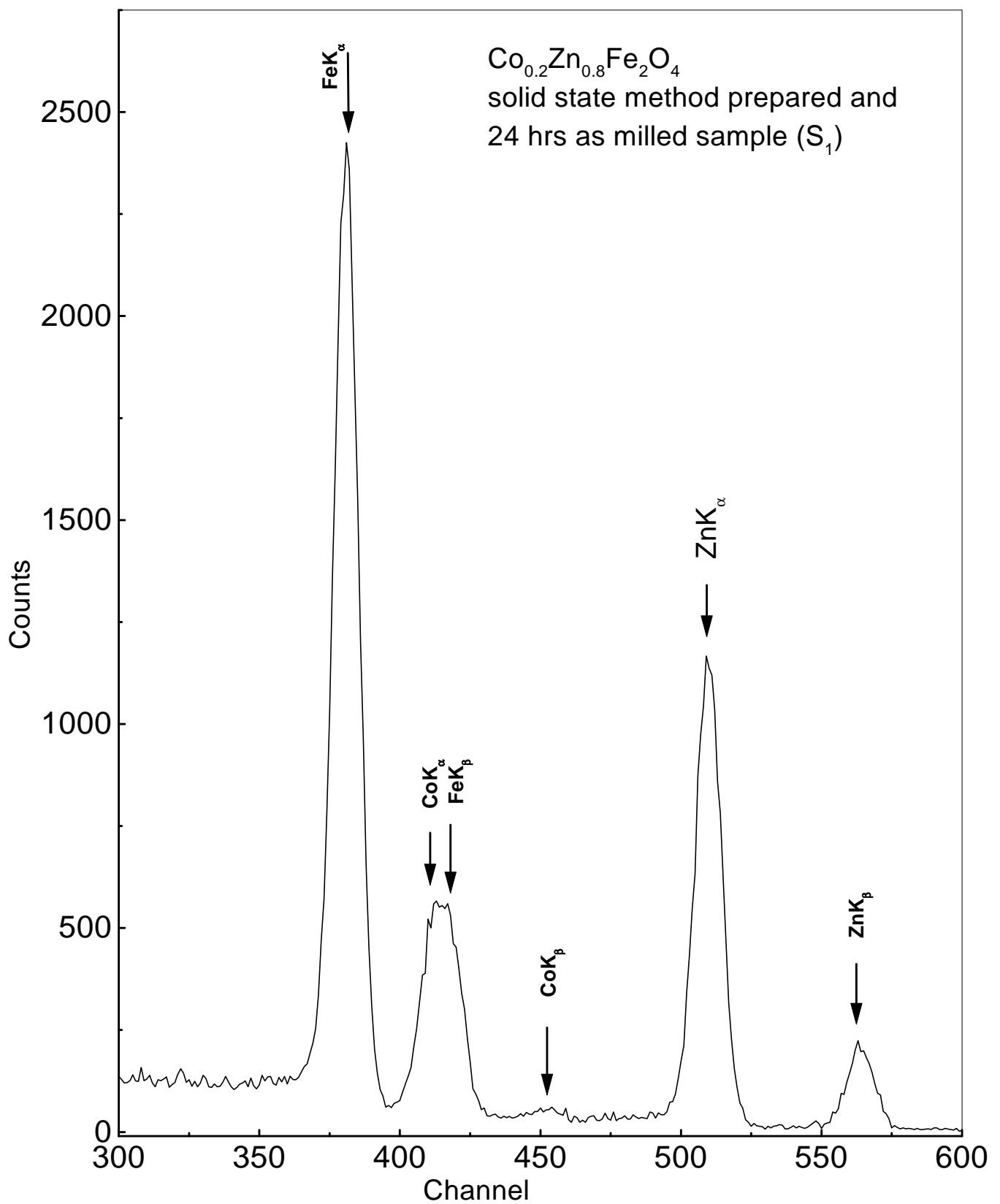


Fig.2 X-ray Fluorescence Spectrum for the as milled sample. The arrow indicate the corresponding metals characteristics  $\text{K}_\alpha$  and  $\text{K}_\beta$  lines.



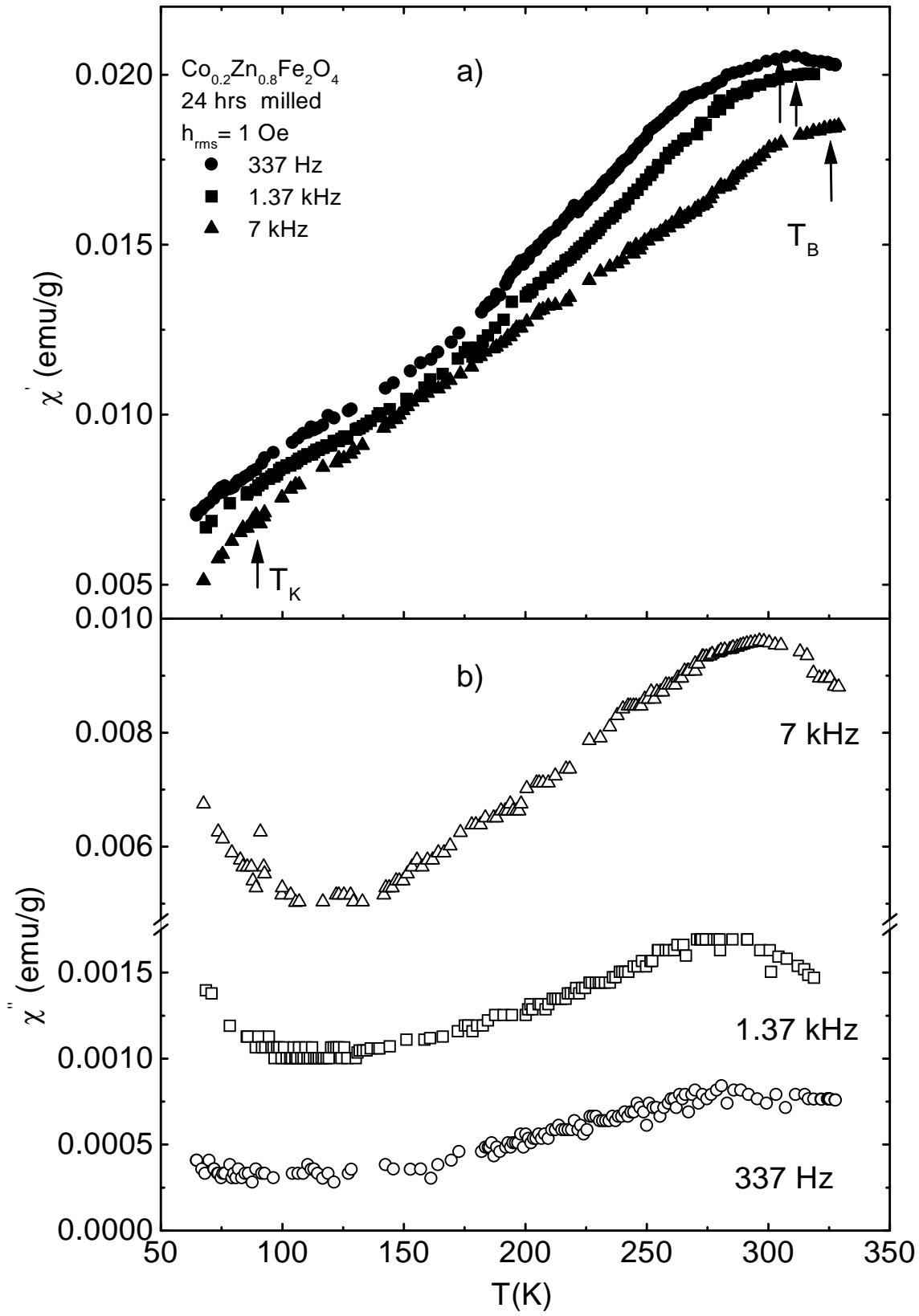


Fig.3 Ac susceptibility  $\chi'$  (in a) and  $\chi''$  (in b) data for as milled sample ( $S_1$ ).  $T_B$  and  $T_K$  represent blocking and spin canting temperature respectively.

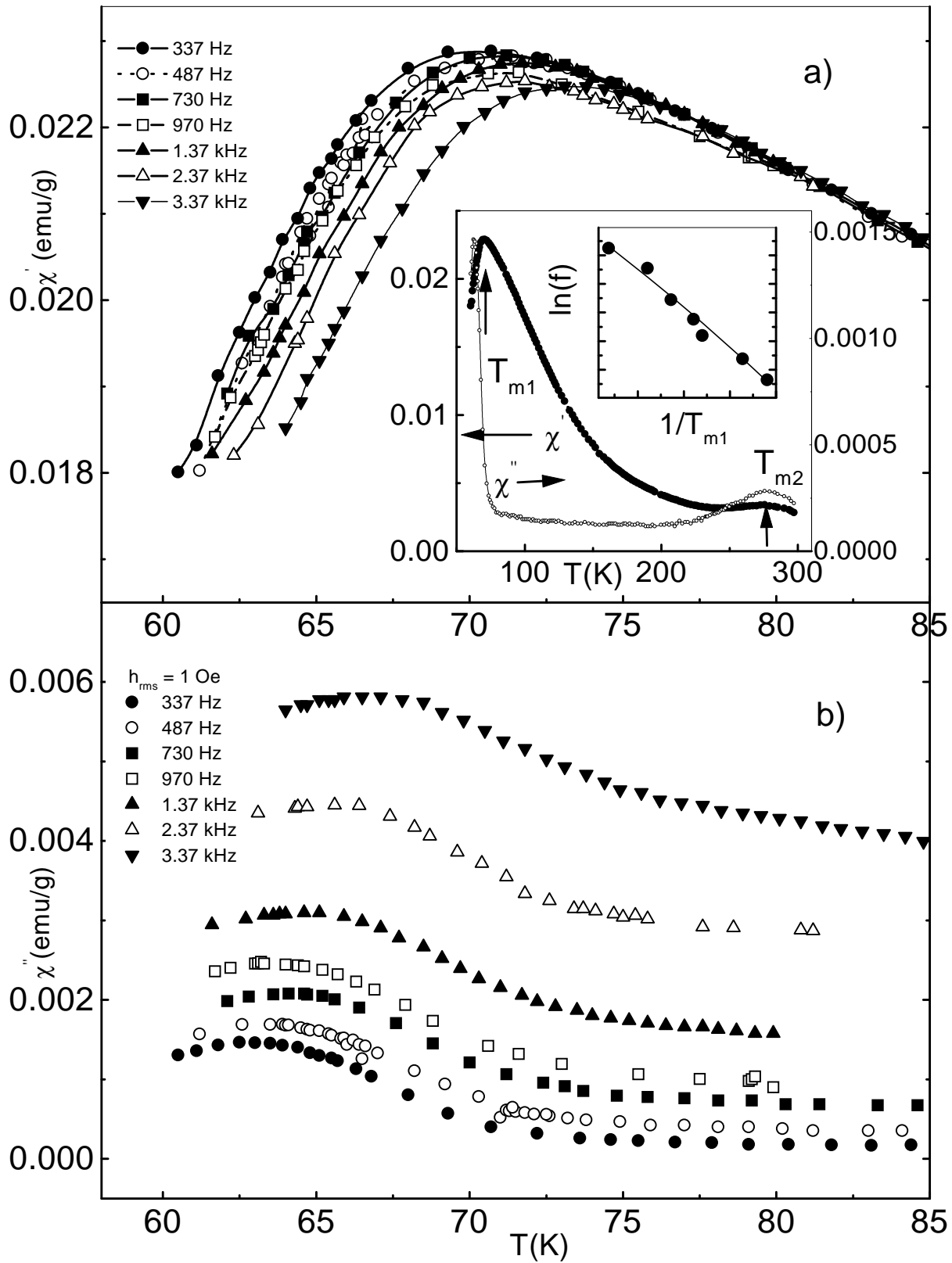


Fig. 4. Ac susceptibility  $\chi'$  (in a) and  $\chi''$  (in b) for the 1000°C- 6 hour heat treated sample ( $S_{N10}$ ). Fig. a insert shows ac susceptibility data at 1 Oe ac field,  $f = 337$  Hz and  $\ln f$  vs  $1/T_{m1}$  plot for the same sample.

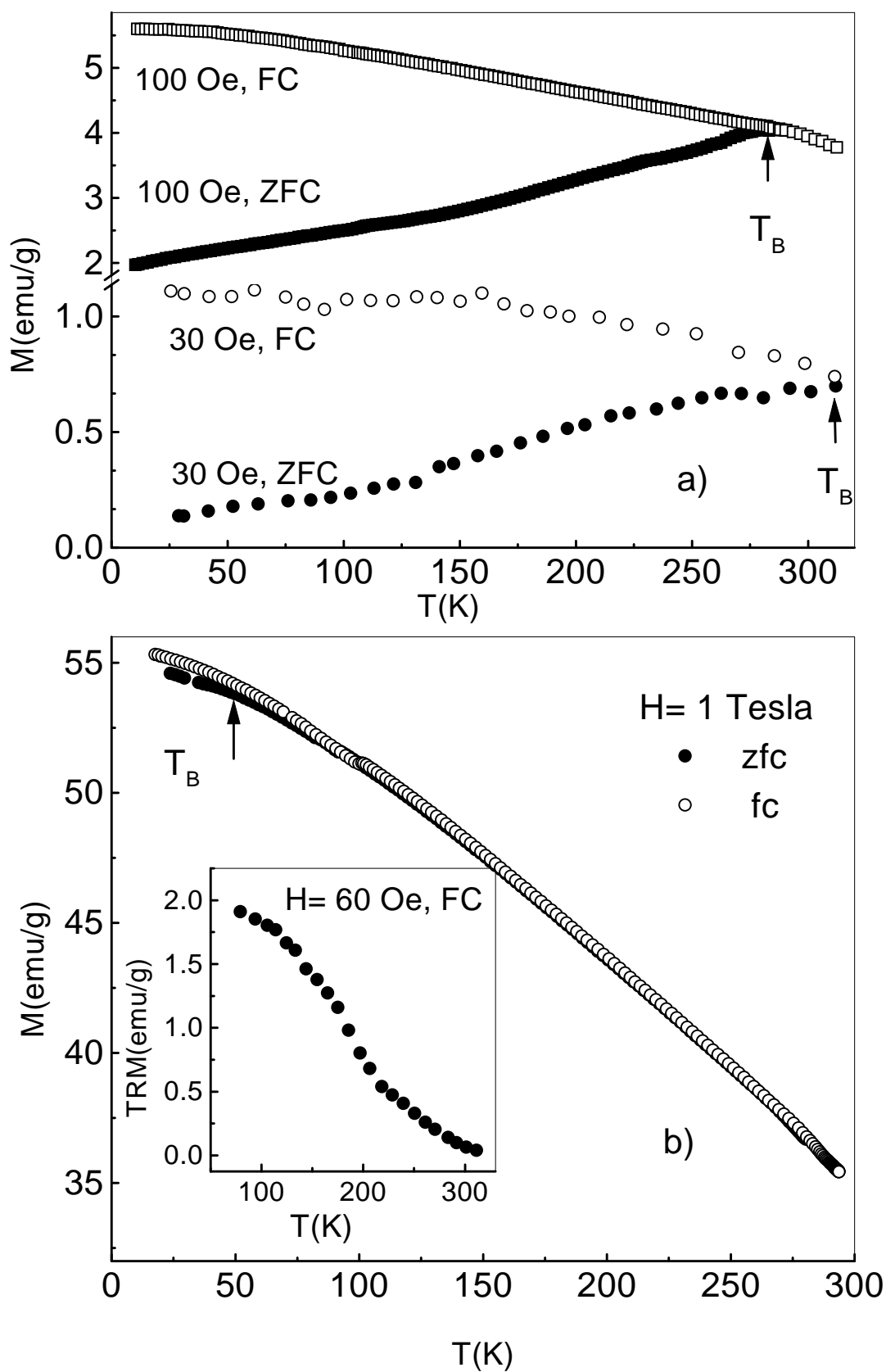


Fig.5 Dc magnetization vs temperature for 24 hrs milled  $\text{Co}_{0.2}\text{Zn}_{0.8}\text{Fe}_2\text{O}_4$  sample. Fig. b inset shows the temperature dependence of field cooled (FC) (cooled in a field of 60 Oe) thermoremanent magnetization (TRM).

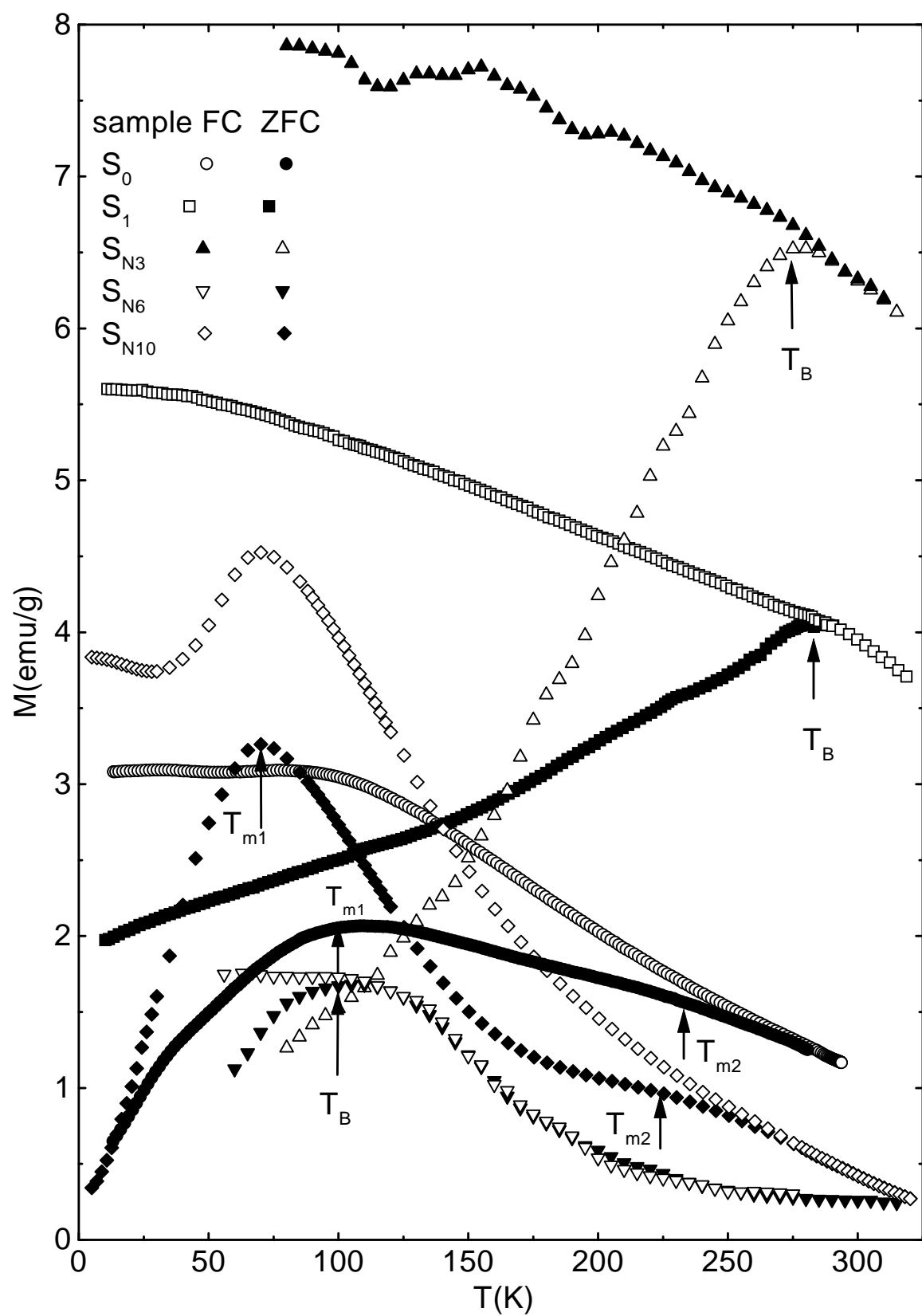


Fig. 6 Temperature dependence of dc magnetization data for different heat treated samples at 100 Oe field.

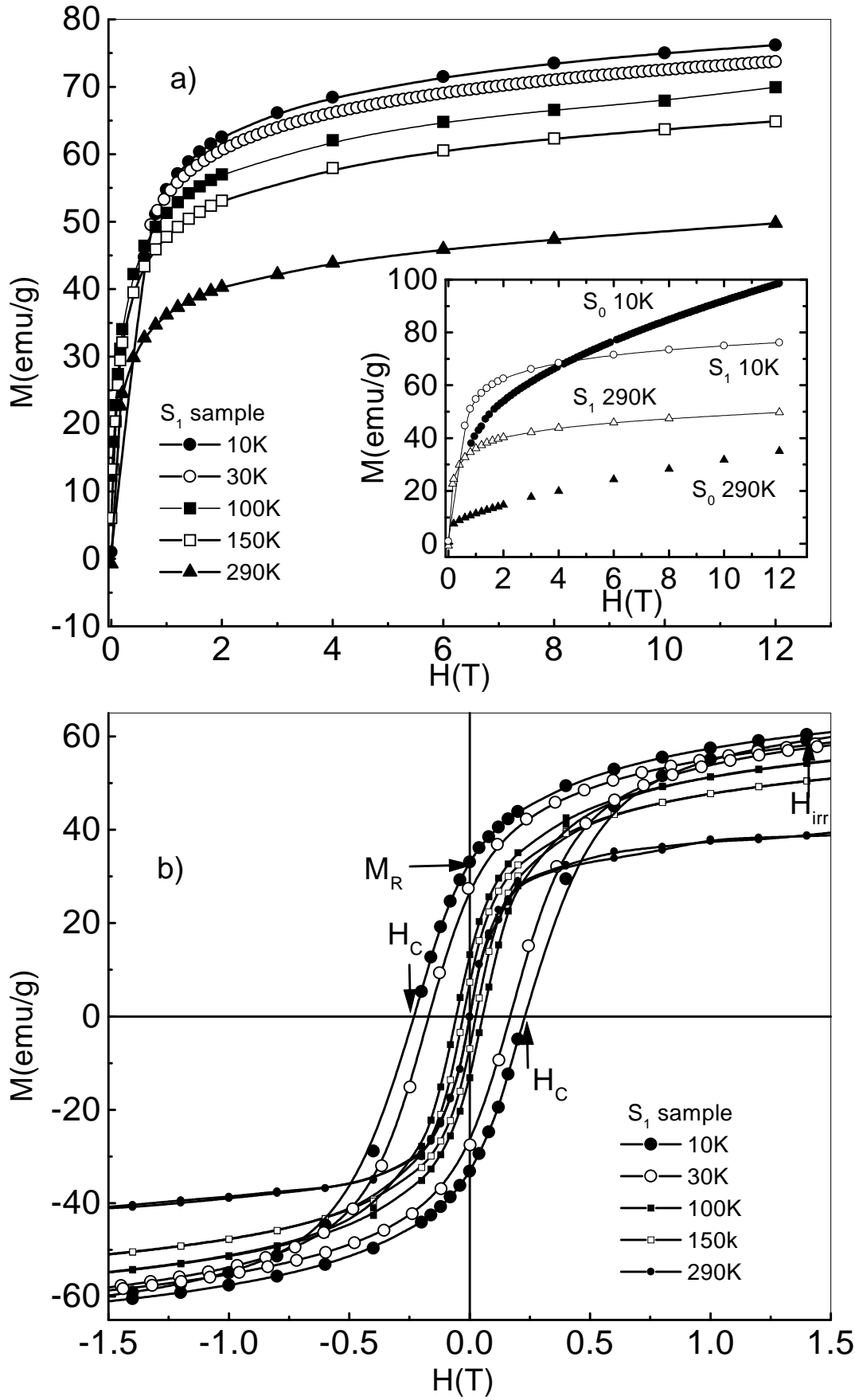


Fig.7 a)  $M$  vs  $H$  plot at different temperatures for  $S_1$  sample and inset Fig. compare the 10K and 290K data of  $S_0$  and  $S_1$  samples.  
b) Hysteresis loops at different temperatures for  $S_1$  sample.  
For  $M_R$ ,  $H_C$  and  $H_{irr}$  see text.

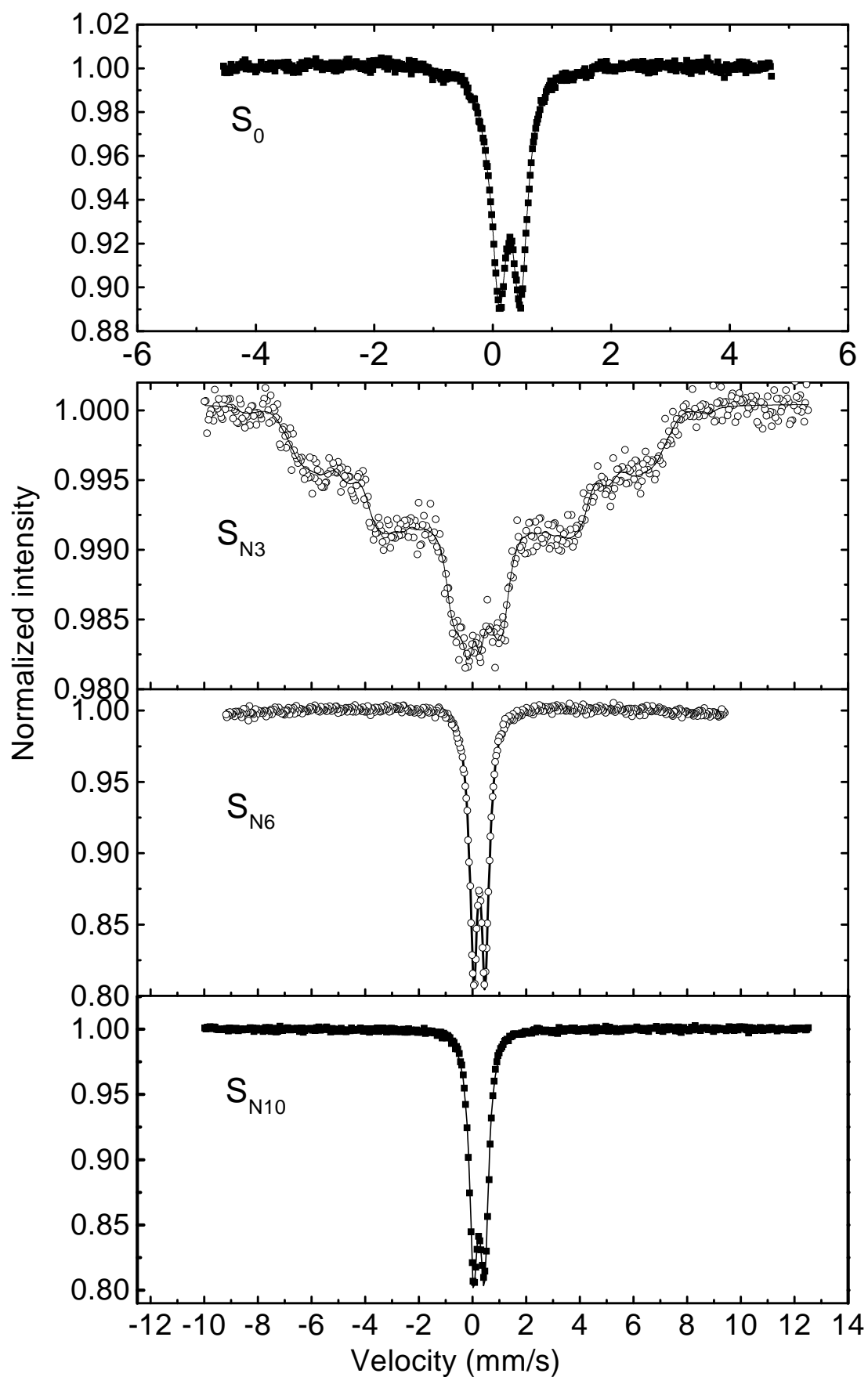


Fig.8 Room temperature Mossbauer spectra recorded in absence of field for as prepared bulk ( $S_0$ ) and heat treated as milled  $S_1$ ,  $S_{N3}$ ,  $S_{N6}$  and  $S_{N10}$  sample.

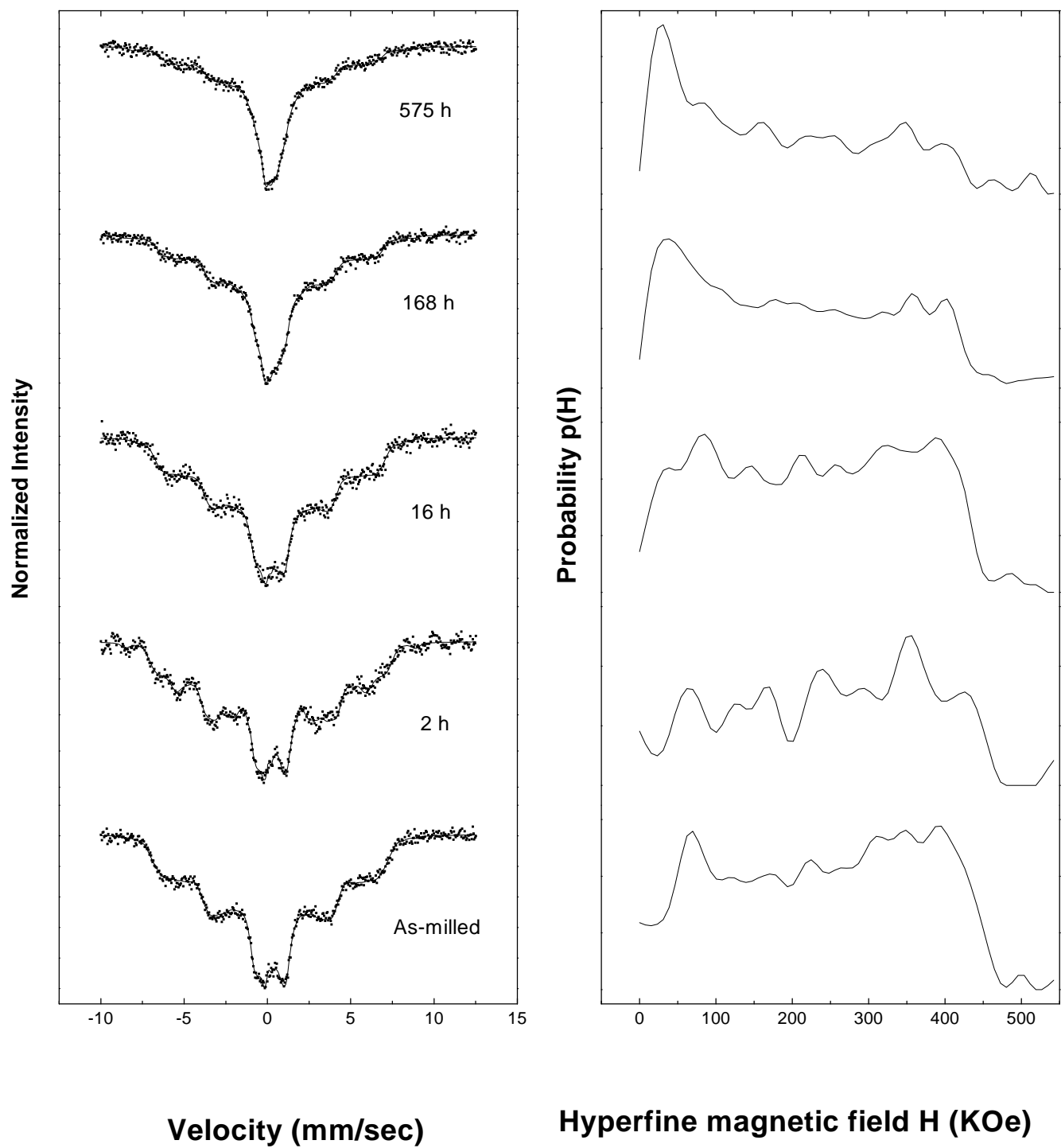


Fig.9 Room temperature Mossbauer spectra for heat treated  $\text{Co}_{0.2}\text{Zn}_{0.8}\text{Fe}_2\text{O}_4$  sample at  $300^\circ\text{C}$  for different time (left) and corresponding hyperfine field distribution (right)

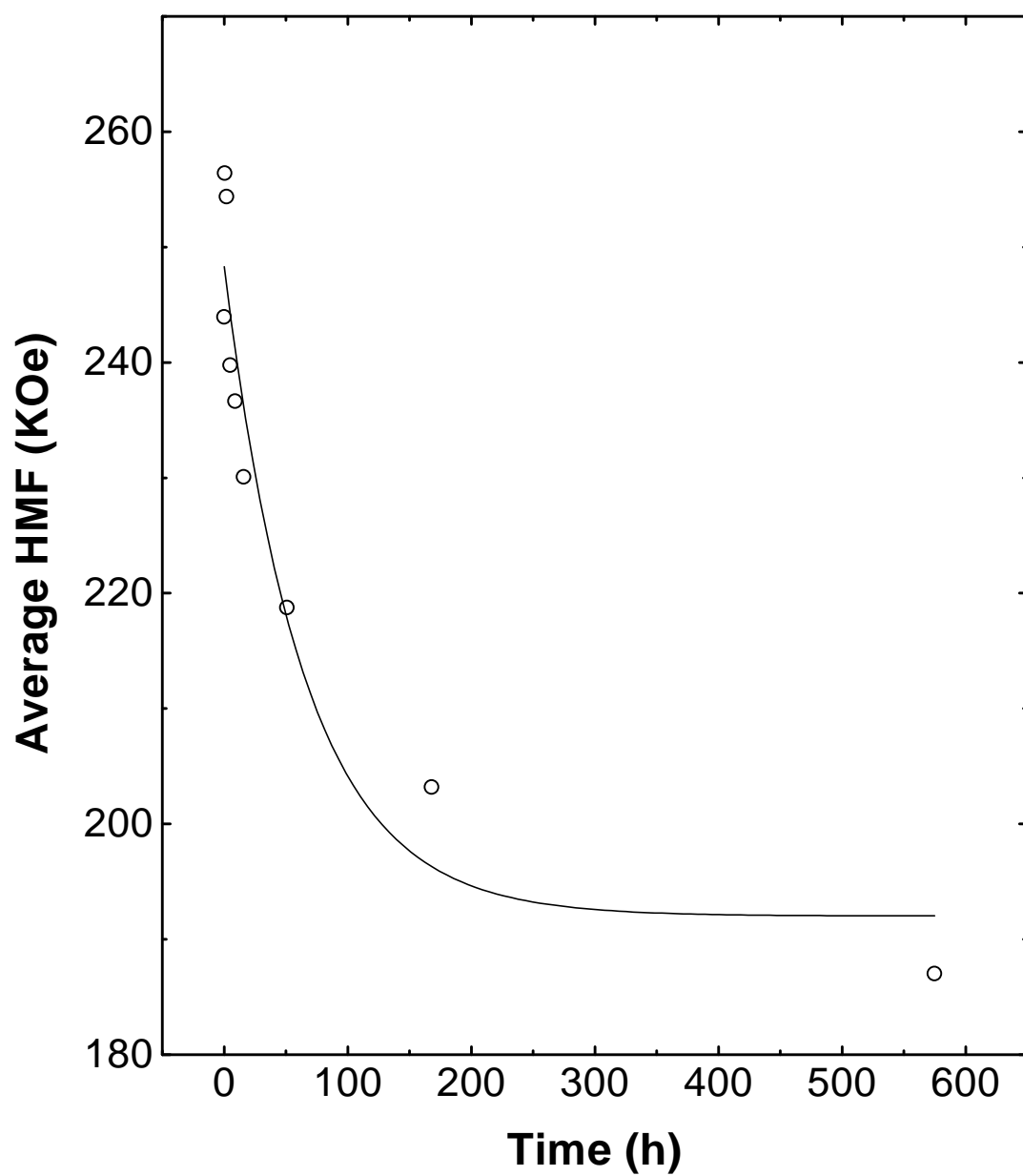


Fig.10 Annealing time (at 300<sup>0</sup>C) dependence of average hyperfine field value as milled for Co<sub>0.2</sub>Zn<sub>0.8</sub>Fe<sub>2</sub>O<sub>4</sub> sample.